Check for updates

Received: 11 October 2022 | Accepted: 17 November 2022

DOI: 10.1002/pamm.202200302

Consideration of chemically-induced damage in a thermo-electrically coupled system

Johanna Waimann[1,2,*], **Tim van der Velden**[2], **Annika Schmidt**[2], **Stephan Ritzert**[2], and **Stefanie Reese**[2]

[1] Modeling and simulation techniques for systems of polycrystalline materials, RWTH Aachen University, Mies-van-der-Rohe-Str. 1, D-52074 Aachen, Germany

[2] Institute of Applied Mechanics, RWTH Aachen University, Mies-van-der-Rohe-Str. 1, D-52074 Aachen, Germany

Electro-chemical machining (ECM) allows the removal of material based on the effect of anodic dissolution and without mechanical contact. Thus, it avoids tool abrasion as well as influencing the surface quality, for instance due to formed dislocations and/or damage. Due to that, ECM is a very attractive machining process for high strength materials such as titanium.

The effect of anodic dissolution is a result of a present electric current in combination with the contact with an electrolyte. We show a material model, which enables to predict the mentioned effect by use of a chemically motivated damage of the material based on Faraday's law. After the approach's introduction, we will address its consideration within a thermo-electrically coupled finite element method by using effective material parameters that differ between metal and electrolyte. The presentation is completed by the numerical results, which show the method's ability to simulate the ECM process.

© 2023 The Authors. *Proceedings in Applied Mathematics & Mechanics* published by Wiley-VCH GmbH.

1 Introduction

Electro-chemical machining (ECM) uses the effect of anodic dissolution and thus enables the processing of even high strength materials without producing undesired effects in the surface layer of the work piece, see [3].

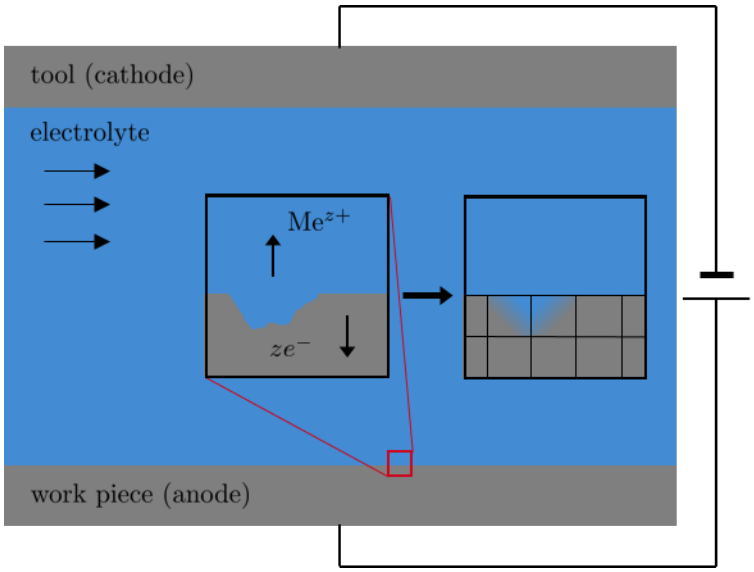

Fig. 1: Sketch of the experimental setup of electrochemical machining and the effective description of anodic dissolution.

The general experimental setup is sketched in Fig. 1: The metallic work piece and tool are connected with a power source and thus serve as anode and cathode. In the gap between them is a flowing electrolyte, which deals as conductor and transports by-products of the chemical reactions away. Due to the current flow and the resulting electro-chemical potential the effect of anodic dissolution takes place. This means that a metal atom Me dissolves into z electrons e^- and an ion Me^{z+}:

$$\mathrm{Me} \rightarrow \mathrm{Me}^{z+} + ze^-. \tag{1}$$

Therein, z is the valency and corresponds to the valence electrons of an atom. The dissolved negative charges then flow in the direction of the positive pole and the positively charged metal ions are transported away by the fluid flow. Further detailed information about the machining process can be found in [4], for instance.

* Corresponding author: e-mail waimann@ifam.rwth-aachen.de, phone +49 241 8025017, fax +49 241 8022001

This is an open access article under the terms of the Creative Commons Attribution-NonCommercial-NoDerivs License, which permits use and distribution in any medium, provided the original work is properly cited, the use is non-commercial and no modifications or adaptations are made.

Up to now, the literature referring to the modeling of this complex multiphysical process is relatively rare. To mention a few of the former works, in [5], the authors use a temperature-dependent multi-ion transport and reaction model to simulate the ECM process considering also the fluid structure interactions. In the phenomenological model in [6], a mathematical equation directly connects the shape of the work piece with the current density at its surface. Finally in [7], the authors propose a highly resolved description for the dissolution of a multiphase structure.

Compared to other works that are often limited to small scale calculations and/or computationally expensive remeshing, we want to propose a homogenized description of the anodic dissolution based on effective material parameters. After this short introduction in the first section, we introduce the effective description in Sec. 2 and its consideration within the electro-thermally coupled boundary value problem in Sec. 3. The numerical results given in the following section (Sec. 4) underline the performance of the proposed method and, with Sec. 5, we conclude the presented work and give a brief outlook.

2 Homogenized description of anodic dissolution

In the following, we refer to the material description introduced by [1] and [2]. As a result of the chemical effect of the anodic dissolution, the material vanishes and is replaced by the electrolyte. Due to the similarities compared to damage modeling, we choose an analogous approach by introducing the dissolution level d which relates the dissolved volume increment $\mathrm{d}V_{\mathrm{dis}}$ to the reference volume increment $\mathrm{d}V_{\mathrm{ref}}$, see also Fig. 2 a). So that, the relation

$$d = \mathrm{d}V_{\mathrm{dis}} / \mathrm{d}V_{\mathrm{ref}} \tag{2}$$

holds. This assumption is chosen in accordance to the well-known variable d in damage mechanics, which can be interpreted as the area of defects divided by the total cross section area [8]. As visualized in Fig. 2 b), the parameter d is for our examined problem of ECM 0 in the metal and 1 in the electrolyte. In the material's surface layer, the chemical reaction takes place and d evolves from 0 to 1.

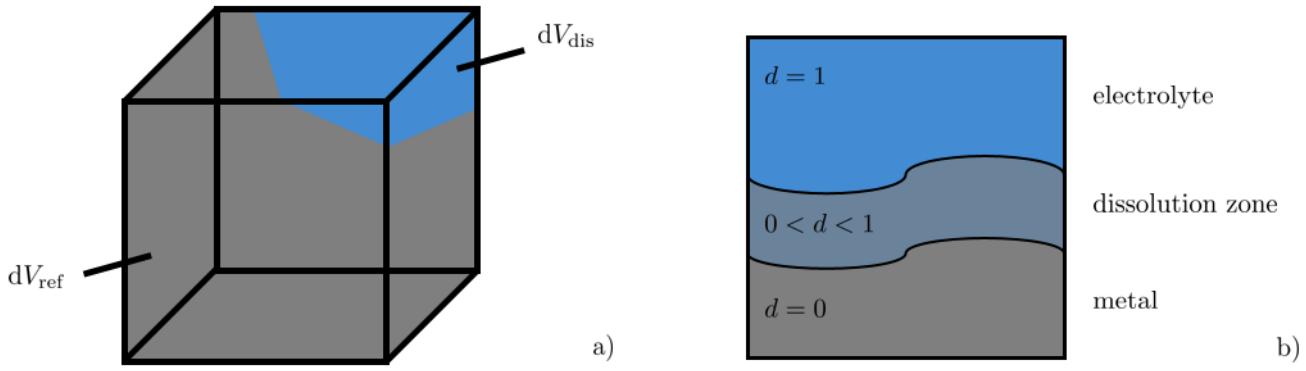

Fig. 2: Partially dissolved volume element (a) and dissolution level d in electrolyte, dissolution zone and metal (b).

The evolution is now described by Faraday's law of electrolysis. Based on works by Harst [9], the evolution equation for the dissolution level reads

$$\dot{d}\,\mathrm{d}V_{\mathrm{ref}} = \mathrm{d}\dot{V}_{\mathrm{dis}} = \nu_{\mathrm{dis}}\,\mathcal{A}\,\mathrm{d}I \tag{3}$$

and hence depends on the experimentally determined material-dependent effective dissolved volume ν_{dis}, the current increment $\mathrm{d}I$ and the activation function $\mathcal{A}$. The latter quantity accounts for the necessary contact between electrolyte and metal. It is thus 1 for the contact case and 0 otherwise. For a more detailed description of the developed method and made assumption, we kindly refer to [1].

3 Thermo-electrical boundary value problem

To simulate the complex ECM process, we consider a thermo-electrically coupled boundary value problem. The resulting boundary value problem depends on two primary variables, the temperature θ and the electric potential v. The heat conduction equation

$$\bar{\rho}_{\mathrm{V}}\bar{c}_{\theta}\dot{\theta} + \mathrm{div}\boldsymbol{q} = \boldsymbol{j}\cdot\boldsymbol{E}, \tag{4}$$

© 2023 The Authors. *Proceedings in Applied Mathematics & Mechanics* published by Wiley-VCH GmbH.

16177061, 2023, 1, Downloaded from https://onlinelibrary.wiley.com/doi/10.1002/pamm.202200302 by Rwth Aachen Hochschulbibliothe, Wiley Online Library on [02/06/2023]. See the Terms and Conditions (https://onlinelibrary.wiley.com/terms-and-conditions) on Wiley Online Library for rules of use; OA articles are governed by the applicable Creative Commons License

in combination with the constitutive equations for the heat flux $\boldsymbol{q}$ and thermal boundary conditions, describes the thermal part of the problem. In Eq. (4), the parameters ρ_{V} and c_θ describe the volume density as well as the heat capacity, $\boldsymbol{j}$ is the electric current density and $\boldsymbol{E}$ the electric field strength. The heat flux consists of two contributions

$$\boldsymbol{q} = -\bar{k}_\theta \mathrm{grad}(\theta) + \bar{\Pi}\boldsymbol{j}. \tag{5}$$

The first summand refers to Fourier's law with the heat conductivity k_θ, the second term accounts for the Peltier effect and serves as an additional coupling to the electrical problem with use of the Peltier coefficient Π.

For the electrical part, the conservation of electric charge

$$\dot{\rho}_{\mathrm{E}} + \mathrm{div}\boldsymbol{j} = 0 \tag{6}$$

holds, in combination with the constitutive equations for the current density $\boldsymbol{j}$ and boundary conditions for v and $\boldsymbol{j}$. In Eq. 6, ρ_{E} refers to the charge density that can be calculated in dependence on the electric displacement field $\boldsymbol{D}$

$$\rho_{\mathrm{E}} = \mathrm{div}\boldsymbol{D} = \mathrm{div}\left(\epsilon_0 \bar{\epsilon}_{\mathrm{r}} \boldsymbol{E}\right), \tag{7}$$

which is a function of the field strength $\boldsymbol{E}$, the electric constant ϵ_0 and the effective relative permittivity ϵ_{r}. The constitutive law for the current density reads

$$\boldsymbol{j} = \bar{k}_{\mathrm{E}} \boldsymbol{E} - \alpha \bar{k}_{\mathrm{E}} \mathrm{grad}(\theta) \tag{8}$$

with the electric conductivity k_{E} and the Seebeck coefficient α. The first contribution considers Ohm's law and the second the coupling to the thermal problem, more precisely the so-called Seebeck effect.

In the aforementioned equations (4) and (7), the material dependent parameters are marked with $\bar{(\cdot)}$. This notation refers to the effective description of the chemical dissolution process. Each parameter is hence calculated by a mixture rule

$$\bar{(\cdot)} = (1-d)\,(\cdot)_{\mathrm{ME}} + d\,(\cdot)_{\mathrm{EL}} \tag{9}$$

and averages the material parameter of the metal $(\cdot)_{\mathrm{ME}}$ and the electrolyte $(\cdot)_{\mathrm{EL}}$, accordingly. This last consideration completes the thermo-electro-chemical method.

Using the test functions $\delta\theta$ and δv, the coupled weak forms read

$$\int_\Omega \left(\bar{\rho}_{\mathrm{V}} \bar{c}_\theta \dot{\theta} - \boldsymbol{j}\cdot\boldsymbol{E}\right) \delta\theta \,\mathrm{d}V - \int_\Omega \boldsymbol{q}\cdot\mathrm{grad}\left(\delta\theta\right)\,\mathrm{d}V + g_{\bar{q}} = 0 \tag{10}$$

$$-\int_\Omega \boldsymbol{j}\cdot\mathrm{grad}\left(\delta v\right)\,\mathrm{d}V + g_{\bar{j}} = 0, \tag{11}$$

wherein $g_{\bar{j}}$ and $g_{\bar{q}}$ include information about the Neumann boundary conditions for the examined body with volume Ω.

Furthermore, we use the time discretization

$$\dot{\theta}^{n+1} = \frac{\theta^{n+1}-\theta^n}{\Delta t}, \quad \dot{v}^{n+1} = \frac{v^{n+1}-v^n}{\Delta t} \tag{12}$$

for the rates of the temperature and the electric potential with the time increment Δt between the two time steps $n+1$ and n. In combination with the finite element discretization into n_{el} elements

$$\Omega \approx \bigcup_{e=1}^{n_{\mathrm{el}}} \Omega^e \tag{13}$$

and the approximation of the test functions as well as the primary variables within each element e using the shape functions $\boldsymbol{N}$

$$\theta^e = \boldsymbol{N}^{\mathrm{T}}\hat{\boldsymbol{\theta}}^e, \qquad \delta\theta^e = \boldsymbol{N}^{\mathrm{T}}\delta\hat{\boldsymbol{\theta}}^e, \tag{14}$$

$$v^e = \boldsymbol{N}^{\mathrm{T}}\hat{\boldsymbol{v}}^e, \qquad \delta v^e = \boldsymbol{N}^{\mathrm{T}}\delta\hat{\boldsymbol{v}}^e, \tag{15}$$

this leads to the finally linearized system of coupled equations

$$\begin{bmatrix} \boldsymbol{K}_{\mathrm{vv}} & \boldsymbol{K}_{\mathrm{v}\theta} \\ \boldsymbol{K}_{\theta\mathrm{v}} & \boldsymbol{K}_{\theta\theta} \end{bmatrix} \cdot \begin{Bmatrix} \Delta\hat{\boldsymbol{v}}^{n+1} \\ \Delta\hat{\boldsymbol{\theta}}^{n+1} \end{Bmatrix} = -\begin{Bmatrix} \boldsymbol{R}_{\mathrm{v}} \\ \boldsymbol{R}_\theta \end{Bmatrix}. \tag{16}$$

© 2023 The Authors. *Proceedings in Applied Mathematics & Mechanics* published by Wiley-VCH GmbH.

16177061, 2023, 1, Downloaded from https://onlinelibrary.wiley.com/doi/10.1002/pamm.202200302 by Rwth Aachen Hochschulbibliothe, Wiley Online Library on [02/06/2023]. See the Terms and Conditions (https://onlinelibrary.wiley.com/terms-and-conditions) on Wiley Online Library for rules of use; OA articles are governed by the applicable Creative Commons License

Therein, $\boldsymbol{K}_{\mathrm{vv}}$, $\boldsymbol{K}_{\mathrm{v}\theta}$, $\boldsymbol{K}_{\theta\mathrm{v}}$ and $\boldsymbol{K}_{\theta\theta}$ are the corresponding tangent matrices and $\boldsymbol{R}_{\mathrm{v}}$ and $\boldsymbol{R}_{\theta}$ are the residuals.

Additional information about the finite element implementation, including the exact formulas for the tangents and the residuals as well as the linearization procedure for the examined problem of electro-chemical machining can be found in [1]. More general information about the finite element implementation of the thermo-electrically coupled problem is given in [10].

4 Numerical results

Figure 3 shows the examined boundary value problem: The simulation setup consists of a metal with an initial irregular roughness, which has contact to an electrolyte. The metal is positively charged by an electric potential v_{an} that varies in time between 0 V and 20 V within 19 load cycles. At the upper boundary, we assume a potential of 0 V. For simplicity, the temperature is held constant at 298.15 K. It thus corresponds to the fluid flow during the pulsed electro-chemical process, which transports the heated fluid and the ions constantly away. For the temperature-dependent approaches of the individual material parameters, we kindly refer to [1].

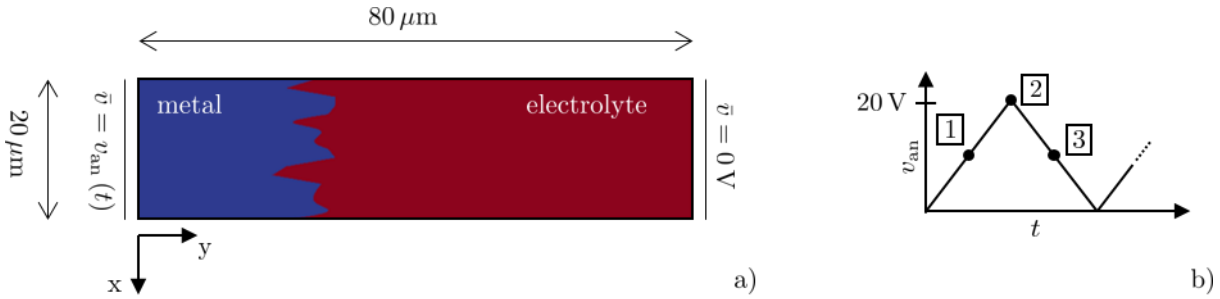

Fig. 3: Numerical simulation of pulsed electro-chemical machining of metal with initial surface roughness: boundary value problem (a) with prescribed varying electric potential at the anode and marked load steps (b).

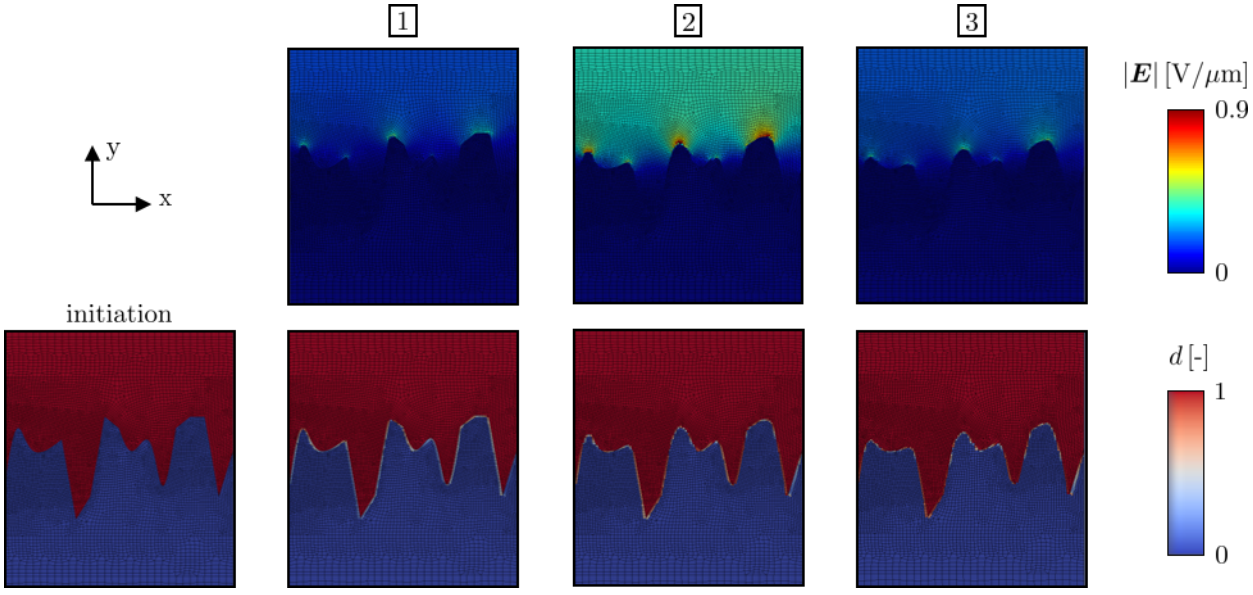

Fig. 4: Numerical simulation of pulsed electro-chemical machining of metal with initial surface roughness: norm of the electric field strength $|\boldsymbol{E}|$ and dissolution level d for three steps during the first load cycle in the surface layer. The load steps are marked in Fig. 3.

The contour plots in Fig. 4 (*right*) show the norm of the electric field strength $\boldsymbol{E}$ (*top*) and the dissolution level d (*bottom*) for the marked steps during the first load cycle, see Fig. 3. The electric field strength is highest at the peaks and thus leads to the flattening of the structure. It can be also seen, that the dissolution is limited to the elements that have contact to the electrolyte, which is a result of the introduced activation function $\mathcal{A}$ in Eq. (3).

© 2023 The Authors. *Proceedings in Applied Mathematics & Mechanics* published by Wiley-VCH GmbH.

16177061, 2023, 1, Downloaded from https://onlinelibrary.wiley.com/doi/10.1002/pamm.202200302 by Rwth Aachen Hochschulbibliothe, Wiley Online Library on [02/06/2023]. See the Terms and Conditions (https://onlinelibrary.wiley.com/terms-and-conditions) on Wiley Online Library for rules of use; OA articles are governed by the applicable Creative Commons License

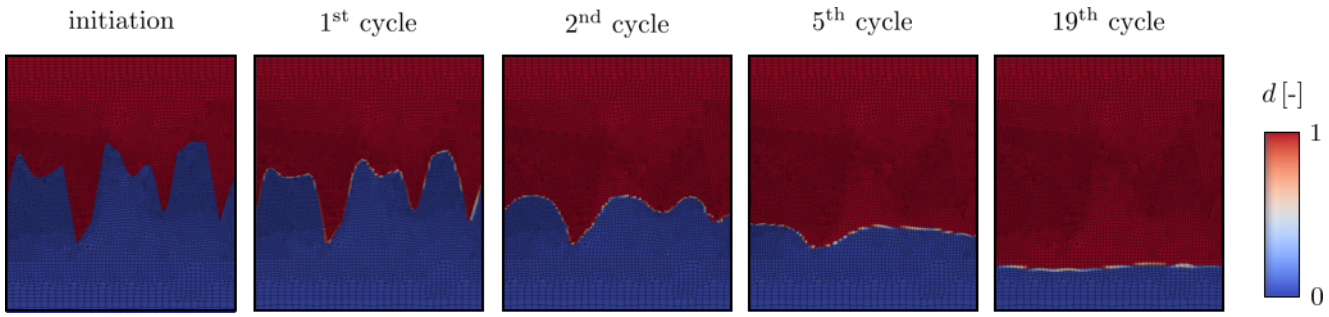

Fig. 5: Numerical simulation of pulsed electro-chemical machining of metal with initial surface roughness: contour plots of the dissolution level d at the initiation, after the 1st, 2nd, 5th and 19th load cycles to show the flattening of the roughness.

The flattening of the surface roughness is also visible in Fig. 5. Therein, the dissolution levels after the 1st, 2nd, 5th and 19th load cycles outline the permanent reduction of the peaks of the initial structure. The surface roughness can be also measured in terms of the quantities Rz and Ra, which have the form

$$Rz = \|y_{\max} - y_{\min}\| \tag{17}$$

$$Ra = \frac{1}{L_{\mathrm{x}}} \int_0^{L_{\mathrm{x}}} \|y(x) - \bar{y}\| \, \mathrm{d}x, \quad \bar{y} = \frac{1}{L_{\mathrm{x}}} \int_0^{L_{\mathrm{x}}} y(x) \, \mathrm{d}x. \tag{18}$$

Therein, Rz just accounts for the maximum and minimum coordinates of the surface. The measure Ra integrates the divergence of each coordinate compared to its average $\bar{y}$ over the whole length of the structure L_{x}. Both quantities are plotted in Fig. 6 over the flown electric charge Q per area A and again show the reduction of the surface roughness during machining. The presented relation is a so-called process signature, which relates a material modification during processing with an inner material load. The development of process signatures for different machining processes is also the aim of the Collaborative Research Center TRR 136 [11], within the framework of which we have carried out our work. Further numerical examples including also a moving cathode in terms of a moving boundary value problem can be found in [1, 2].

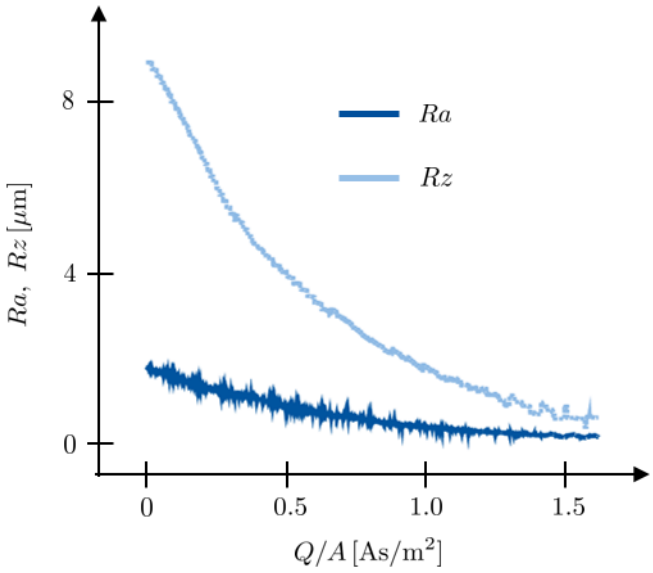

Fig. 6: Numerical simulation of pulsed electro-chemical machining of metal with initial surface roughness: surface roughness measures Ra and Rz over flown electric charge Q per area A (process signature).

5 Conclusion and Outlook

With this work, we propose an effective formulation for the chemical process of anodic dissolution during electro-chemical machining. Instead of a discrete consideration of the modified surface roughness, we introduce a dissolution level, which

© 2023 The Authors. *Proceedings in Applied Mathematics & Mechanics* published by Wiley-VCH GmbH.

16177061, 2023, 1, Downloaded from https://onlinelibrary.wiley.com/doi/10.1002/pamm.202200302 by Rwth Aachen Hochschulbibliothe, Wiley Online Library on [02/06/2023]. See the Terms and Conditions (https://onlinelibrary.wiley.com/terms-and-conditions) on Wiley Online Library for rules of use; OA articles are governed by the applicable Creative Commons License

enables a homogenized description of the chemical reaction. Furthermore, we showed its consideration within a thermo-electrically coupled boundary value problem by use of material parameters which take into account the mixture of electrolyte and metal as well as the resulting weak form and its finite element implementation. The presented numerical example of a pulsed machining of an initially irregular surface roughness shows the ability of the developed method to display the complex surface modification.

In our future works, we would like to extend the model to account for polycrystalline and multiphase structures. With that we want to examine the influence of different dissolution velocities on the resulting surface roughness. In addition to that, we will work on the mesh dependency due to the introduced activation function by use of a smoother formulation of the complex problem. The consideration of further chemical reactions, e.g. at the cathode, as well as a fluid structure interaction deal as additional topics for future investigations.

Acknowledgements The work is funded by the Deutsche Forschungsgemeinschaft (DFG, German Research Foundation) – Projektnummer 223500200 – TRR 136. We gratefully acknowledge the financial support of the subproject M05. Open access funding enabled and organized by Projekt DEAL.

References

[1] T. van der Velden, B. Rommes, A. Klink, S. Reese, and J. Waimann, Int. J. Solids Struct. **229**, 111106 (2021).
[2] T. van der Velden, S. Ritzert, S. Reese, and J. Waimann, arXiv:2202.12704 (2022).
[3] T. Bergs, and S. Harst, CIRP Annals **69**, 153-156 (2020).
[4] F. Klocke, M. Zeis, T. Herrig, S. Harst, and A. Klink, Procedia CIRP **24**, 114-119 (2014).
[5] D. Deconinck, S. Van Damme, J. Deconinck, Electrochimica Acta **69**, 120-127 (2012).
[6] J. Kozak, and M. Zybura-Skrabalak, Procedia CIRP **42**, 101-106 (2016).
[7] F. Klocke, S. Harst, M. Zeis, and A. Klink, Procedia CIRP **68**, 505-510 (2018).
[8] L. M. Kachanov, Introduction to Continuum Damage Mechanics (Martinus Nijhoff Publishers, Dordrecht, 1986), p. 4-6.
[9] S. Harst, Entwicklung einer Prozesssignatur für die elektrochemische Metallbearbeitung (Apprimus Wissenschaftsverlag, Aachen, 2019).
[10] J. L. Pérez-Aparicio, R. L. Taylor, and D. Gavela, Comp. Mech. **40** (1), 35-45 (2007).
[11] E. Brinksmeier, S. Reese, A. Klink, L. Langenhorst, T. Lübben, M. Meinke, D. Meyer, O. Riemer, and J. Sölter, Nanomanuf. Metrol. **1** (4), 193-208 (2018).

© 2023 The Authors. *Proceedings in Applied Mathematics & Mechanics* published by Wiley-VCH GmbH.

16177061, 2023, 1, Downloaded from https://onlinelibrary.wiley.com/doi/10.1002/pamm.202200302 by Rwth Aachen Hochschulbibliothe, Wiley Online Library on [02/06/2023]. See the Terms and Conditions (https://onlinelibrary.wiley.com/terms-and-conditions) on Wiley Online Library for rules of use; OA articles are governed by the applicable Creative Commons License